Dynamical Coupling of a Battery Electro-Thermal Model and the Traction Model of an EV for Driving Range Simulation

Ronan German, Seima Shili, Anatole Desreveaux, Ali Sari, Pascal Venet, Alain Bouscayrol

Dynamical Coupling of a Battery Electro-Thermal Model and the Traction Model of an EV for Driving Range Simulation at Various Ambient Temperatures

R. German[1,3], S. Shili[2], A. Desreveaux[1,3], A. Sari[2], P. Venet[2], A. Bouscayrol[1,3]

[1] Univ. Lille, Centrale Lille, Arts et Métiers Paris Tech, HEI,
EA 2697 – L2EP - Laboratoire d'Electrotechnique et d'Electronique de Puissance, F-59000 Lille, France
[2] Univ Lyon, Université Claude Bernard Lyon 1, Ecole Centrale de Lyon, INSA Lyon, CNRS, Ampère, F-69100 Villeurbanne, France
[3] MEGEVH, French network on hybrid and electric vehicles, France
Contact author: ronan.german@univ-lille.fr

Abstract— The driving range of electric vehicles is a sensitive issue. In simulation, this range is determined by coupling a battery model and a traction model of the vehicle. But most of the battery models used for such studies are generally without temperature dependence on the electrical parameters. In this paper, a battery electro-thermal model is dynamically coupled with the traction model of a studied electric vehicle. Simulation results are provided to show the impact of the temperature on the driving range. The initial battery model (without temperature dependence) leads to an overestimation of the driving range of 3.3% at -5°C and an underestimation of 2.5% at 40°C.

***Index Terms*— Electric Vehicle; System Modelling; Li-ion Battery; Characterization; Electro-Thermal Modelling.**

Table 1 Parameters and symbols

	Parameter	Name	Value	Unit
Cell	Cell capacity	c_{AhCell}	>160	A.h
	Cell nominal voltage	$u_{CellNom}$	3.3	V
	Maximal cell discharge current	i_{Cell}	480	A
	Cell interconnection resistance	R_{Con}	505	μΩ
	Cell weight	---	5.6	kg
	Cell thermal resistance	R_{ThCell}	2.63	K/W
	Cell thermal capacitance	C_{ThCell}	2430	J/K
Battery	Battery config. (series x parallel)	n_{SCells} x n_{PCells}	24 x 1	cells
	Battery nominal voltage	u_{BatNom}	79.2	V
	Battery nominal power	p_{Bat}	38.0	kW
	Battery mass	m_{Bat}	134	kg
EV traction	Aerodynamic drag coefficient	c_X	0.35	---
	Front surface	S	1.55	m²
	Air volumic mass	φ_{Eq}	1.3	kg/m³
	Road friction	f_0	150	N
	Wheel radius	r_{Wheel}	0.26	m
	Reduction coefficient	k_{Red}	5.84	---
	Mechanical efficiency	η_{Mech}	0.85	---
	Electric drive peak power	$P_{DriveMax}$	25	kW
	Electric drive efficiency	η_{Drive}	[1]	---

I. INTRODUCTION

Electric vehicles (EVs) are a solution for balancing the petroleum depletion and reducing the global carbon emissions. Nevertheless, the long charging time and the reduced driving range are frequent worries for future EV owners [2].

Characterization studies showed that a cold temperature has a strong impact on the electrochemical energy storage in a battery [3][4][5]. The battery capacity fades and the resistance increases at low temperature. In addition, the temperature affects the aging of the battery [6], [7].

As a consequence many studies focus on the battery thermal behaviour for use in electric vehicles.

-1) Some allow thermal simulation with fixed electrical parameters. That means that, even if the battery model is electro-thermal the electrical and the thermal part are not coupled (except for the heat power coming from the electrical part) [8][9] .

-2) Some are focused on the characterization of electrical parameters at different temperature but no coupling is done with a traction chain[10][11][12][13]. In that case the battery model is coupled to a current source. An interesting approach has been recently developed for battery modelling in cold weather. In [10] a battery electro-thermal model has been developed based on multi-temperature characterizations.

-3) Some are coupling the traction chain of the vehicle with a partly temperature dependent electric model of battery (only OCV for [14]) but impedence parameters are not dependent of temperature. This lack of temperature dependence for impedence parameters will underestimate the current consumption in low temperature.

The novelty of this paper is a better estimation of the impact of the temperature on driving range for a coupled electro-thermal battery model [10] by the coupling it with the traction chain [14]. It improves back [14] by adding the full electrical parameters dependence developed in [10]. With the proposed coupled electro-thermal-traction model current has to adapt to the electrical parameters in order to achieve the same velocity profile under different temperature and State of Charge (SoC) conditions.

The validation is original as it is not performed in hardware in the loop with a vehicle simulator programm [15] [14] or with a fixed recorded current cycle [10]. It is performed with measures during a real driving cycle in a real vehicle.

Moreover, this paper presents the model in Energetic Macroscopic representation. Contrary to [14] [10] [11], no

derivative is used. All the equations are reorganized with integrals. This respects the physical causality (output delayed compare to input).

This paper is limited to the impact of the battery temperature on the driving range. Anciliaries systems supplied by the battery are known for significantly increasing the battery current consumption (heating [16] [17] and air conditioning [18][19]). They are not considered in this paper.

In section II the coupled electro-thermal battery model is organized in a causal way to be coupled with the traction subsystem model of the studied EV. In section III, a cell used in the battery of the studied EV is characterized at several temperatures. In section IV, the battery model is validated at the system level with measurements on board the EV. In section V, the impact of the temperature on the driving range is studied with simulation.

II. Causal Organization of the EV Model

A. Electro-thermal model for one cell

The electric model (Fig. 1) is a classical equivalent circuit model composed of 3 parts [4]:

- The Open Circuit Voltage (OCV_{Cell}) is linked to the energy stored by electrochemical mechanisms (OCV_{Cell} increases with the state of charge SoC).
- The series resistance (R_{SCell}) represents the sum of the conduction, the ionic transport in electrolyte and the charge transfer resistances. The double-layer capacitance is neglected given the time constants considered (greater than few seconds).
- The phenomena related to the insertion and the diffusion of the ions in the battery nanostructure is represented by a $R_{DiffCell}//C_{DiffCell}$ parallel equivalent circuit instead of a Warburg impedance as in [20]. This model is a compromise between accuracy and computation time for embedded systems [10].

In classical approaches, the dependence on the SoC is generally taken into account on the OCV. It is less usual to find internal temperature effect on electrical parameters (T_{Int}) [14].

In this paper, the chosen electrical model (Fig. 1) includes full SOC and temperature dependence of all the electrical parameters [10] contrary to [21].

The Peukert effect (i.e. the dependence of the battery recoverable capacity with discharge current rate) can be neglected for the LFP battery technology (Peukert constant between 0.99 and 1.04)[22]. LFP stability with current rate is confirmed by previous works [23].

The thermal model of the battery (*Fig. 2*) is a standard averaged thermal model built with the following hypothesis [24]:

- The thermal capacitance of the cell core (the inside part of the cell) C_{ThCell} is taken into account. The thermal capacitance of the cell surface is neglected as its package is very lightweight compared to the core.
- The equivalent thermal resistance r_{ThCell} represents the heat transfers between the core to the surface (conduction) and the surface to the air (convection).

The heat power (P_{Heat}) is supposed to come only from the joule effect in R_{SCell} and $R_{DiffCell}$ (1).

$$P_{Heat} = R_{SCell}.i_{Cell}^2 + R_{DiffCell}.i_{RDiffCell}^2 \quad (1)$$

As in [10] the electrical and thermal part of the model are coupled by the internal temperature and the heat power (Fig. 3).

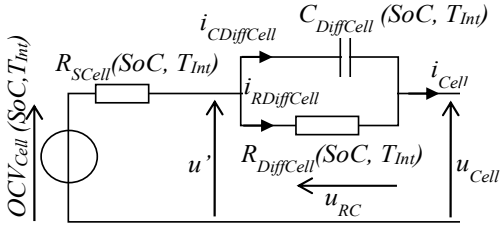

Fig. 1 Structure of the electric model for one cell

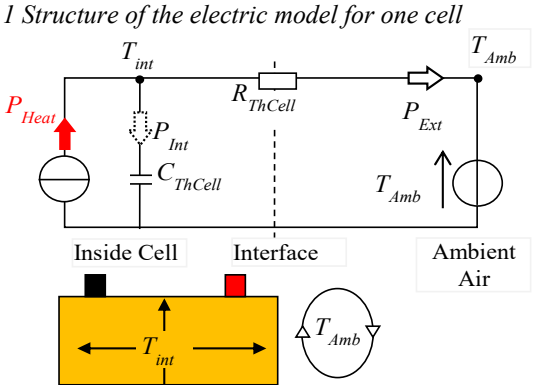

Fig. 2 Structure of the thermal model for one cell [21]

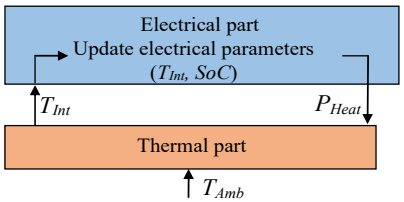

Fig. 3 Electro-thermal coupling principle

B. EMR of the cell electro-thermal model

In order to highlight the coupling of the electrical and the thermal parts of the cell model, the EMR (Energetic Macroscopic Representation) formalism is used. It will enable later an easy coupling of the battery model with the traction subsystem model.

EMR [25] is a functional and graphical description using pictograms (see Annex A). EMR highlights the power exchange between different multi-domain elements by the action reaction variables. In that way, the product of the action and reaction variables leads to the instantaneous power. Moreover, EMR is based on the causality principle. With causality, the output can only be an integral function of the inputs (see *Fig. 4*), i.e. the output can only be a consequence of the inputs, i.e. the outputs is obtained after a delay from the input changes.

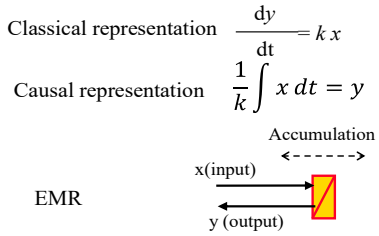

Fig. 4 From classical representation to EMR

In [10], the electro-thermal model is not organized according to the causality principle. In order to better understand the interaction between the thermal and electrical parts, this model is reorganized in a causal way using EMR (*Fig. 5*). This new organization will enable an easy coupling with the traction subsystem model later.

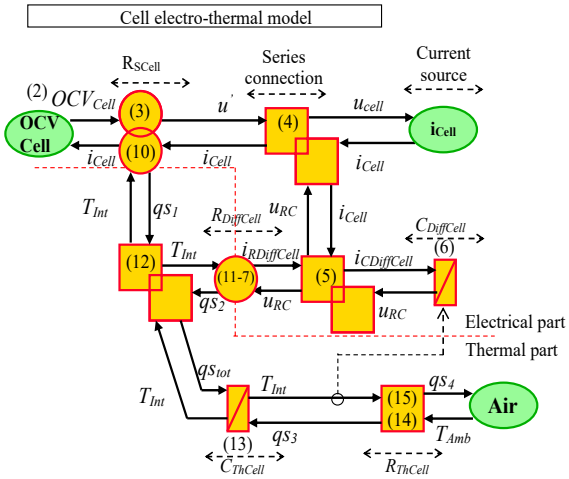

Fig. 5 EMR of the dynamical electro-thermal model[21]

The SoC is calculated from the integration of the current, the initial SoC and the discharge capacity of the cell (2).

$$SoC(\%) = SoC_{Init} - \frac{100}{3600.C_{AhCell}}.\int_0^{t_{Ch/Dch}} i_{Cell}\,dt \quad (2)$$

OCV_{Cell} is represented as a source of voltage in EMR (green oval). The resistance R_{SCell} is represented as a conversion element as there is no delay (integral) between inputs and outputs (3).

$$OCV_{Cell} - R_{SCell}.i_{Cell} = u' \quad (3)$$

The series connection is a coupling element i.e. distribution of energy (4).

$$u' - u_{RC} = u_{Cell} \quad (4)$$

The parallel connection (current node) is also a coupling element (5).

$$i_{Cell} - i_{RDiffCell} = i_{CDiffCell} \quad (5)$$

$C_{DiffCell}$ is an accumulation element i.e. storage of energy (6).

$$u_{RC} = \frac{1}{C_{DiffCell}}\int_0^t i_{CDiffCell}\,dt \quad (6)$$

$R_{DiffCell}$ is a conversion element i.e. energy conversion without storage (7).

$$i_{RDiffCell} = \frac{u_{RC}}{R_{DiffCell}} \quad (7)$$

The thermal part is reorganized to represent the effort and the flow variables (Fig. 6).

For thermal modelling, the effort variable is the temperature (K) and the flow variable is the entropy flow q_S (in W/K). The power P is achieved by multiplying those two variables (8):

$$P = q_S.T \quad (8)$$

The entropy flows coming from R_{SCell} (9) and $R_{DiffCell}$ (10) are summed with a coupling pictogram (11):

$$q_{SRSCell} = \frac{R_{SCell}.i_{Cell}^2}{T_{Int}} \quad (9)$$

$$q_{SRDiffCell} = \frac{R_{DiffCell}.i_{RdiffCell}^2}{T_{Int}} \quad (10)$$

$$q_{STot} = q_{SRSCell} + q_{RDiffCell} \quad (11)$$

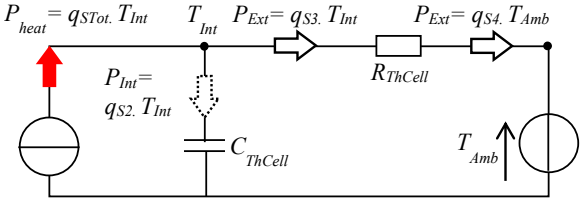

Fig. 6 Flow and effort variables for thermal model [21]

The thermal capacitance is an accumulation element as there is a differential equation (12). With the works of ludovic Horrein [16], this equation is reorganized for EMR, by making appar the flow and the effort variables (13) and with the integral causality (14). $T_{IntInit}$ is the initial internal temperature of the cell. It is supposed to be equal to the ambient temperature.

$$\frac{dT_{Int}}{dt} = \frac{P_{Int}}{C_{ThCell}} \quad (12)$$

$$\Leftrightarrow \frac{dT_{Int}}{dt} = \frac{(q_{STotCell} - q_{S3}).T_{int}}{C_{ThCell}} \quad (13)$$

$$\Leftrightarrow T_{Int} = T_{IntInit}.e^{\frac{1}{C_{ThCell}}\int_0^t (q_{STotCell} - q_{S3})dt} \quad (14)$$

The ambient air is considered as a source of temperature. The thermal resistance is a conversion element (15), (16).

$$q_{S3} = \frac{T_{Int} - T_{Amb}}{(R_{ThCell}).T_{Int}} \quad (15)$$

$$q_{S4} = \frac{T_{Int} - T_{Amb}}{(R_{ThCell}).T_{Amb}} \quad (16)$$

As R_{SCell} and $R_{DiffCell}$ are present in the thermal and the electrical parts, they are represented as multi-physical (electro-thermal) converters.

All the electrical parameters (OCV_{Cell}, R_{sCell}, $R_{DiffCell}$, $C_{DiffCell}$) are depending both on the internal temperature and on the SoC of the cell. The thermal parameters are constant (they are related to geometry and mass of the cell).

C. *Building the battery model*

The battery of the studied EV is composed of 24 cells in series. For mass repartition purpose, the battery is divided into 3 modules (7/10/7 cells). They are placed at different locations (2 under the seats and one under the front hood). In a module, the cells are placed in line and separated by cooling holes (Fig.

7). The corresponding battery model is built with the two following assumptions:

- There is no parameters dispersion between the cells.
- The cooling holes make the thermal interactions between the cells negligible. As a consequence the thermal part of the cell model is considered unchanged in this particular EV battery.

These strong assumptions will be validated by comparisons between simulation and experimental measurement on the vehicle (see section IV).

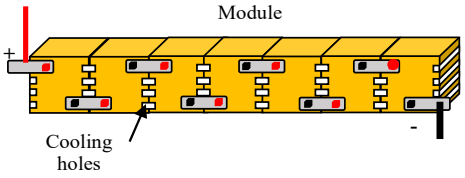

Fig. 7 Module 1 setup in the studied EV [21]

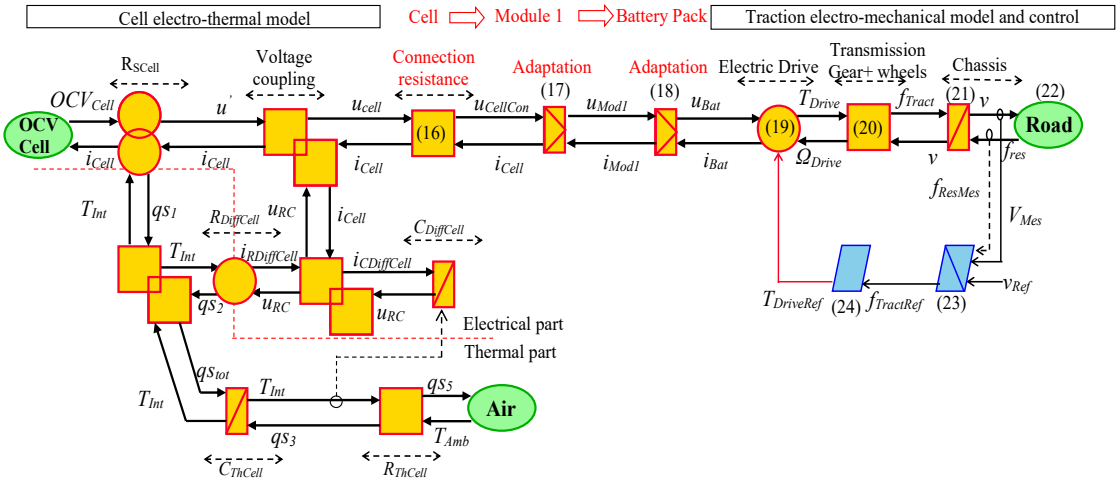

Fig. 8 EMR of the Tazzari Zero with control

The value of the connection resistance between cells has been estimated to R_{Con}=505 µΩ onboard the vehicle with a current peak and the corresponding voltage drop during driving the studied EV. It is considered constant during the test. A conversion pictogram (17) is added to the cell EMR (Fig 8).

$$u_{Cell} - R_{Con}.i_{Cell} = u_{CellCon} \tag{17}$$

Where $u_{CellCon}$ is the voltage for one cell with connections. The electrical model is deduced from the cell model (18). In EMR it corresponds to an adaptation element i.e. power amplification.

$$\begin{cases} u_{CellCon}.7 = u_{Mod1} \\ i_{Cell} = i_{Mod1} \end{cases} \tag{18}$$

Where u_{Mod1} and i_{Mod1} are the module voltage and current. Then a second adaptation element is added (see Fig. 8) to build the battery model (19).

$$\begin{cases} u_{Mod1}.\dfrac{24}{7} = u_{Bat} \\ i_{Mod1} = i_{Bat} \end{cases} \tag{19}$$

Where u_{Bat} and i_{Bat} are the battery voltage and current.

D. Integration of the battery model in the EV model

The EV used for the test is a Tazzari Zero [26]. This is a two-seats urban electric car. Its parameters can be found in Table 1. A global efficiency map has been derived from measurements [1], including the electric drive efficiency (n_{Drive}). Equations (20)-(23) are organized in a causal way to be included in the global EMR (see Fig. 8).

Electric Drive

$$i_{Bat} = \eta_{Drive}^{k} \frac{\Omega_{drive}.T_{drive}}{u_{Bat}} \tag{20}$$

k=1 if traction mode
k=-1 if regenerative braking

Transmission

$$\begin{cases} T_{Drive}.k_{Drive}.\dfrac{1}{r_{Wheel}}. = f_{Tract} \\ \Omega_{Drive} = \dfrac{1}{r_{Wheel}}.k_{Drive}.v \end{cases} \tag{21}$$

Chassis

$$v = \frac{1}{M_{Tot}} \int_0^t f_{Tract} - f_{Res} dt \tag{22}$$

Road

$$f_{Res} = f_0 + \frac{1}{2} c_x S \varphi_{Air} v^2 \tag{23}$$

Where Ω_{Drive} and T_{Drive} are the electric drive speed, and torque. Ω_{Wheel} and T_{Wheel} are the speed, and torque at the wheel. f_{Tract} and f_{Res} are the traction and resistive forces. v_{Veh} is the velocity of the vehicle. Other parameters are defined in Table 1.

The electric drive is a multi-physical (electro-mechanical) converter (20), the mechanical transmission is a mono-physical converter (21) and the chassis is an accumulation element (22). The road is a source of resistive forces (23). EMR allows to settle the control structure by a mirror effect (24), (25).

The velocity control is achieved by the inversion of the chassis and the transmission in order to provide the right reference torque to the electric drive ($T_{DriveRef}$) in order to follow the velocity reference (v_{Ref}). The control pictograms are represented in blue in Fig. 8.

Inv. Chassis
$$f_{TractRef} = f_{ResMes} + C(s).(v_{Ref} - v_{Mes}) \quad (24)$$

Inv. Transmission
$$T_{DriveRef} = \frac{r_{Wheel}}{k_{Drive}}.f_{TractRef} \quad (25)$$

III. Characterization of One Cell

A. Electrical Characterization

The electrical parameters of the cell are dependent with temperature. Consequently they are characterized every 15 °C. The characterization temperature range (-5 °C, 55 °C) is an acceptable range of temperature for EV battery in temperate countries [27]. The characterization protocol is composed of 4 steps and repeated for all the characterized temperatures.

1. Recharge @ 25 °C: in order to begin systematically with the same amount of stored energy the initial charge is made after a minimal rest (i.e. i_{Cell}= 0A) of 8h at 25°C. The recharge method is a constant current/ constant voltage with a cutoff voltage of 4V. The cutoff current is 8A (C/20). This allows to have a reproducible reference *SoC* (100 %) at the end of this step.

2. Characterization temperature stabilisation: the cell is put at rest and the temperature is settled at the characterization temperature at least 8h to equalize the cell internal temperature with the characterization one.

3. Pseudo OCV characterization: the discharge/ charge is achieved at low C-rate (C/10 = 16 A).

4. Pulse characterization: the impedance parameters of the electrical model are characterized at different *SoC* levels with current pulses (+/-1C). The *SoC* selected levels are 90 %, 70 %, 50 %, 30 % and 10 %.

With the pseudo-OCV characterization, the charge and discharge capacity can be extracted (26):

$$C_{AhCell} = \frac{1}{3600}\int_0^{t_{Ch/Dch}} |i_{Cell}|dt \quad (26)$$

C_{AhCell} is the cell capacity (A.h). $t_{Ch/Dch}$ is the total charge or discharge time to achieve the full charge or discharge (from 2.8 V to 4.0 V). The capacity C_{AhCell} versus temperature evolution is presented in Fig. 9. The capacity increases with the temperature as in [5]. Above 25 °C, the maximal measured capacity (192 A.h) is reached. This value is 20% higher than the rated one (160 A.h). It might correspond to the margin of the manufacturer to provide at least 160 A.h capacity during the whole lifespan of the cell [28].

OCV_{Cell} = f (*SoC*) is also characterized during the pseudo-OCV characterization . Indeed, at low current the measured cell voltage u_{Cell} is near from OCV_{Cell}. A small difference is noticeable for OCV_{Cell} during charge and discharge (Fig. 10). This phenomenon is due to the battery OCV hysteresis [29].

During the pulse characterization (Fig. 11), a double characterization pulse inspired from the HPPC method [30]. Although the chosen characterisation method, is leading to uncertainties on parameters it is chosen for its simplicity, its reproducibility and because the current rates implied are near from the real use of the cells in the EV. (+/- 1C) is applied during 10 s (Fig. 11). For the sake of simplification, the extracted parameters (27)-(29) are an average between charge and discharge characterization pulses. The parameters for calculation are defined in Fig. 11.

$$R_{SCell} = \frac{\Delta U_{Cell1s}}{\Delta i_{Cell}} \quad (27)$$

$$R_{DiffCell} = \left|\frac{\Delta U_{Cell1s} - \Delta U_{Cellr}}{\Delta i_{Cell}}\right| \quad (28)$$

$$C_{DiffCell} = \frac{\tau_{Diff}}{R_{DiffCell}} \quad (29)$$

$$\Delta U_{RC} = |\Delta U_{Cellr} - \Delta U_{Cell1s}| \quad (30)$$

Fig. 12 shows the evolution of the impedance parameters as a function of ambient temperature and SoC. For 0 % and 100 % SoC, the parameters are extrapolated. The series resistance R_{SCell} represents the equivalent effect of the terminals, the transports of the ions in the electrolyte and the charge transfer mechanisms. When the temperature increases, the electrolyte viscosity decreases and the ions movement is easier [31].

Thus, R_{SCell} is decreasing with the temperature and it is independent of the SoC (see Fig. 12).

At low SoC the positive electrode is nearly saturated with lithium. Thus, the insertion and diffusion of ions is more difficult causing more concentration gradient (increase of $R_{DiffCell}$). The diffusion capacitance $C_{DiffCell}$ increases with SoC and temperature.

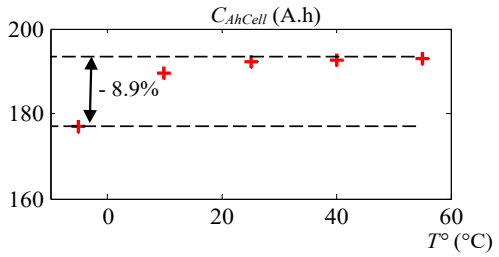

Fig. 9 Evolution of capacity with ambient temperature

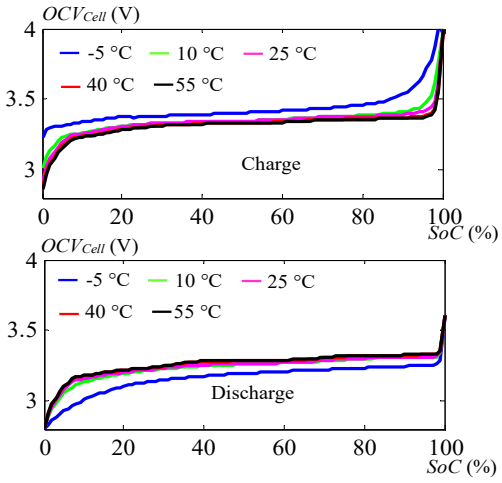

Fig. 10 OCV vs. SoC and temperature

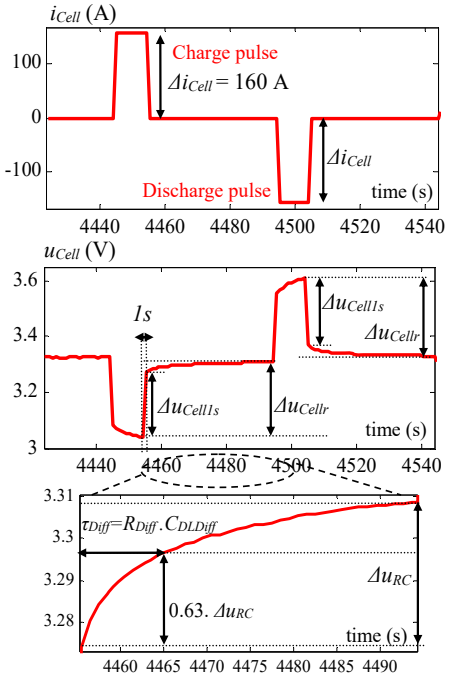

Fig. 11 Characterization pulses

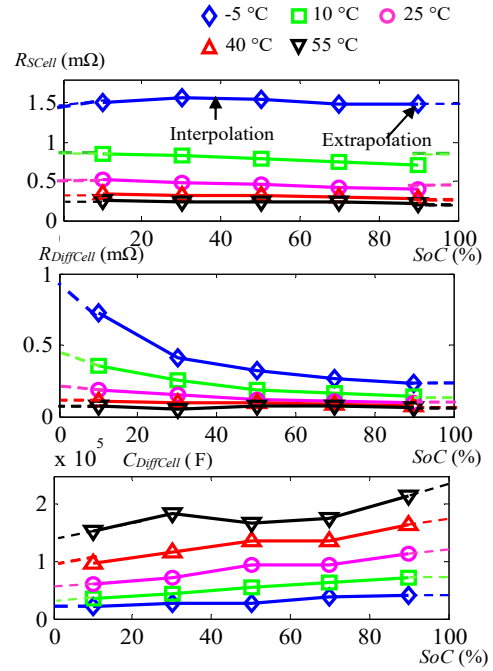

Fig. 12 Impedance parameters with SoC and temperature

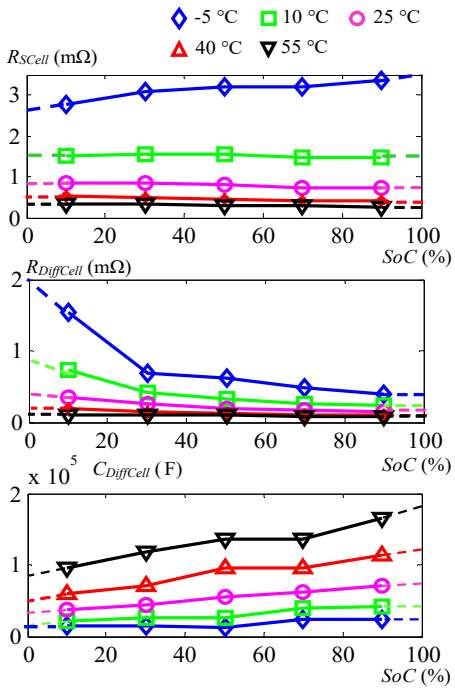

B. *Thermal characterization*

The thermal parameters are characterized at 25 °C. They are mainly related to the mass of the cell and the thermal exchange surface (independent on the ambient temperature).

The internal temperature of the tested cell is recorded on the terminals with thermocouples (closest accessible points to the averaged internal cell temperature [24]). Indeed, terminals are linked to the core of the cell by metallic foils with high thermal conductivity. The ambient temperature of the air around the cell is recorded by a supplementary thermocouple. The cell is placed in a thermal chamber. The temperature is settled at 25 °C for 8h in order to equalize the cell internal temperature (T_{Int}) with the ambient temperature. Then the characterization process presented in Fig. 13 is applied.

At first, a characterization current (+/- 160 A) is applied until the temperature T_{Int} is stabilized (self-heating step) [24].

The stabilised temperature difference (ΔT_{Stab}) can be measured. This step is used to identify the value of the R_{ThCell}.

$$R_{ThCell} = \frac{\Delta T_{stab}}{P_{Heat}} = 2.60\ K.W^{-1} \quad (31)$$

Then the characterization current is turned off and the temperature T_{Int} is decreasing (cooling step). The extraction of the thermal time constant τ_{Th} is achieved (see Fig. 13). The thermal capacitance is extracted with (4):

$$C_{ThCell} = \frac{\tau_{Th}}{r_{ThCell}} = 2.43\ 10^{3}\ J.K^{-1} \quad (32)$$

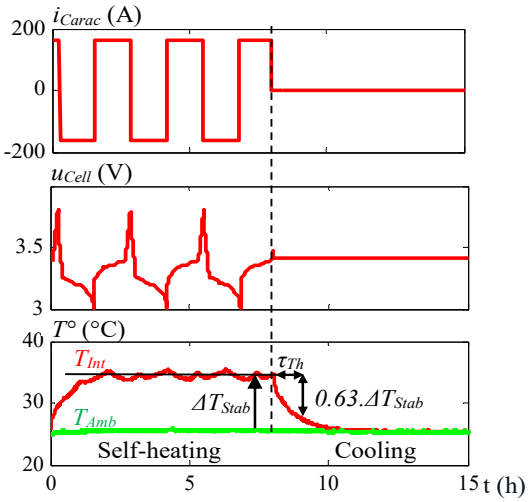

Fig. 13 Thermal characterization protocol

IV. VALIDATION OF THE MODEL

A. *Validation at the cell level (subsystem level in laboratory)*

The tested EV has been instrumented with voltage sensors, current sensors and thermocouples. The cell current is recorded during a real driving cycle on a campus [32]. As the velocity is limited to 30 km/h on the campus, the current as a function of time is moderate (Fig.14.a).

In a second time, in a laboratory, the real current cycle is applied to one cell with a high-power programmable supply (0-30 V -200/+200A) until the minimal cell voltage (i.e. 2.8 V) is reached (Fig.14.b). The experimental cell voltage (u_{Cell}) and temperature (T_{Int}) are recorded. The test is performed for 4 ambient temperatures (-5 °C, 10 °C, 25 °C, 40 °C) in a thermal chamber.

The experimental results ($u_{CellExp}$, T_{IntExp}) are compared to the simulation outputs ($u_{CellSim}$, T_{IntSim}) for the same input, i.e. the current of the cycle. Two models are considered:

- the classical model with the parameters characterized at 25°C (Param @25°C),
- The second model with the characterizations at different temperatures to update the electrical parameters.

Contrary to [33], no adaptive observer is used to adapt the value of parameters. For illustration purpose, the cell voltage evolution is presented as a function of time for an ambient temperature of - 5 °C (Fig. 14.b). The red curve corresponds to the experimental data, the black one to the classical model and the blue one to the temperature-dependent model

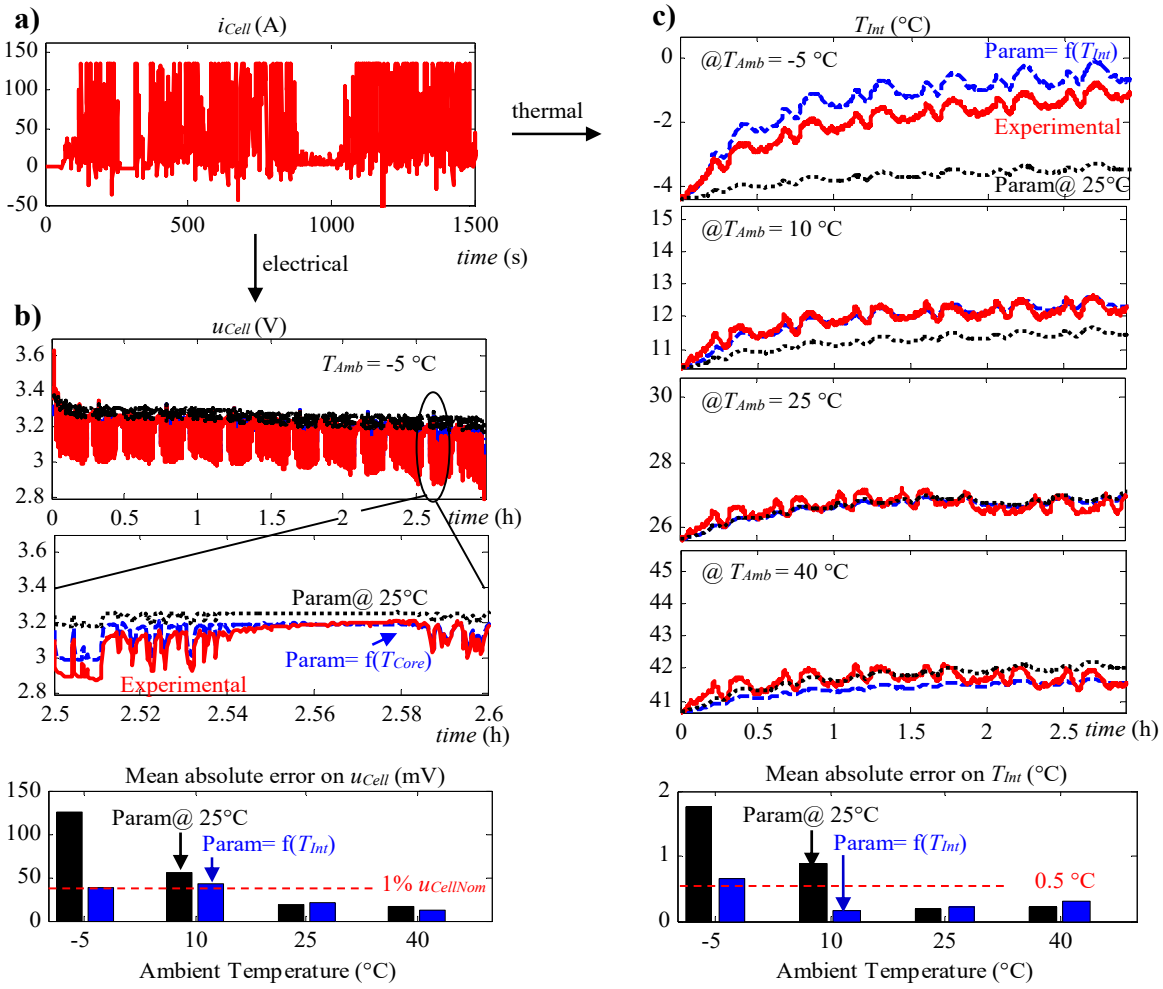

Fig. 14 Real EV current (a) used for electrical (b) and thermal (c) validations of cell model

Taking into account the impact of temperature on electrical parameters brings more accuracy for cell voltage dynamical and static behaviour at low temperature.

The mean absolute error on voltage is then quantified with (33) for different temperatures.

$$Error = \frac{1}{N_S}\sum_{1}^{N_S}\left|u_{CellExp} - u_{CellSim}\right| \quad (33)$$

where N_S is the number of samples during the test.

The model including temperature dependence leads to a an average error on u_{Cell} (~1%) compared to $u_{CellNom}$ (3.3V) at any temperature (Fig. 14.b). The use of a HPPC type characterisation and no correction (by adaptative filter for instance) leads to uncertainty on the impedance parameters. As a consequence, the most part of the average error occurs when current peaks (thus voltage drops) are high (see the zoomed part in Fig. 14.b). When the current is near from 0 (from 2.54 h to 2.58 h in Fig. 14.b) the experimental voltage of the cell and the voltage of the coupled electro thermal model are the same. That means that the pseudo OCV is estimated with lower error than u_{Cell} by the model. On the contrary, using the parameters characterized at 25 °C induces a 124 mV (3.8% compared to the 3.3 V nominal voltage) error at -5 °C. The error is increasing when temperature is decreasing because of the decrease of the capacity and the increase of the series and diffusion resistances.

Fig. 14.c presents the evolution of cell temperature for different ambient temperatures.

The mean absolute error (34) is also presented:

$$Error = \frac{1}{N_S}\sum_{1}^{N_S}\left|T_{IntExp} - T_{IntSim}\right| \quad (34)$$

For low temperatures (up to 10 °C) the temperature on electrical parameters affects the accuracy of the temperature estimation (Fig. 14.c). The maximal error is 1.7 °C at – 5°C. For temperatures higher than 25 °C the effect of the temperature on the electrical parameters has lower impact.

B. Validation at the system level

This section aims to validate the battery electro-thermal model at the system level (on-board tests on the real EV). That means that the full vehicle model (coupling the battery with the traction system) is tested here.

The tested EV is instrumented. The sensors are recorded while driving:

- the battery current (i_{BatExp}),
- the ambient temperature around the battery (T_{AmbExp}) and the battery voltage (u_{BatExp}),
- the temperature on one terminal of one cell in the battery ($T_{TermExp}$).
- The vehicle velocity.

The EV is driven for 6000s. A new velocity cycle is recorded (Fig. 15) outside the campus. This cycle is applied as a reference for the simulation (Fig. 8).

The experimental results and the proposed dynamical coupled EV model simulation results are compared for thermal (Fig. 16) and electrical (Fig. 17) behaviors. The measured temperature ($T_{TermExp}$) is influenced by the internal temperature of the cell. Indeed, the terminals are linked to the core of the cell by aluminium foils (high thermal conductivity). The connection temperature also influences $T_{TermExp}$.

As the cell mass is much higher than the connection the cell thermal behaviour is slower compared to the connection one. As a consequence the internal temperature (T_{IntEst}) is estimated by a low pass filter on on the measured terminal temperature.

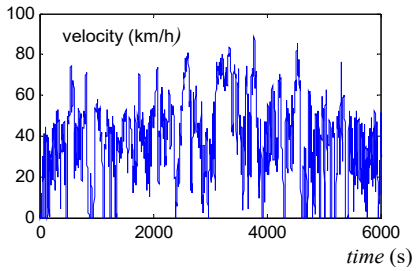

Fig. 15 Recorded velocity of the tested EV

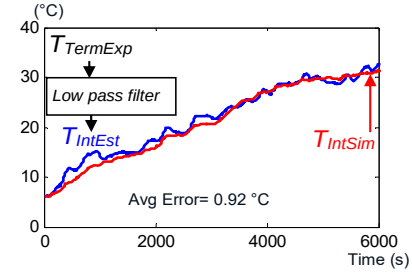

Fig. 16 Experimental and simulated battery temperature

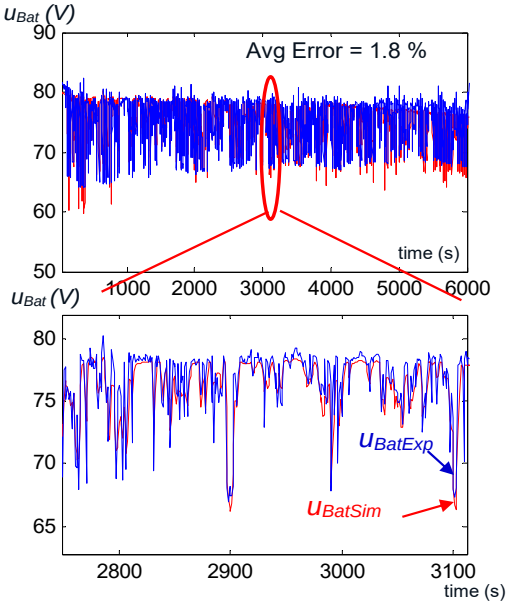

Fig. 17 Experimental and simulated battery voltage

The comparison shows negligible errors on the battery thermal and electrical behaviors. Of course, the chosen assumptions of the battery electro-thermal model depend on the pack architectures, the cells and the studied EV. For the chosen vehicle, all cells are assumed identical and not thermally influenced by the surrounding cells. However, acceptable simulation results are obtained with averaged errors of 0.92 °C for internal temperature and 1.8 % on battery voltage.

V. Interest of the Electro-Thermal-Traction Dynamical Coupled Model

The right approach to obtain the driving range of a vehicle is to couple a battery model with the studied EV traction model (simulation at the system level). As a consequence the validated EV model as presented in section IV.B is used. The reference cycle is a velocity cycle (see Fig 8).

Thus, two battery models are studied:

- For the battery classical electrical model the electrical parameters are fixed to their values at 25°C (Fig. 1)
- For the electro-thermal coupled model the electrical parameters are dependent on the battery internal temperature (T_{Int}).

The WLTC driving cycle (Fig. 18) is applied to the full EV model including its velocity control (Fig. 8). Although simulation results are dependent on the model precision, all the input parameters can be settled and reproduced. This is not possible by driving in real life.Thus, the simulation on a validated model is a good way to compare the influence on one factor (the battery model used in the EV model (Fig. 19) , or the ambient temperature (Fig. 20)) on the system.

When the EV traction is coupled, the current is adapted from the battery voltage in order to achieve the same velocity cycle. The resistive part of the model are influenced by cold temperatures(Fig. 12).

As a consequence, the current consumption is higher at low temperature for the proposed model (Fig. 19). The driving range is influenced by 5.9 % between -5 °C and 45°C ambient temperature (Fig. 20). The classical electrical battery model overestimates by 3.3% the driving range at -5 °C and underestimates it by 2.5% at 40°C.

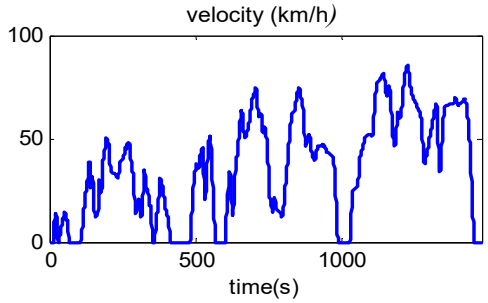

Fig. 18 WLTC driving cycle

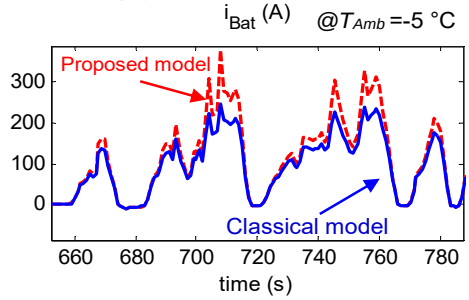

Fig. 19 Battery current at -5°C

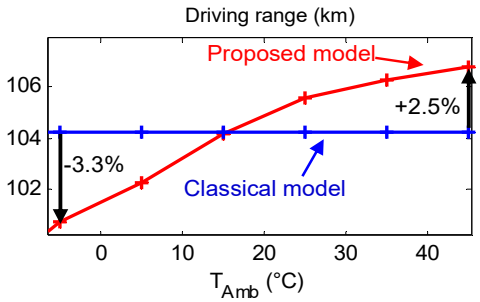

Fig. 20 Driving range as a function of ambient temperature

VI. Conclusion

A recent electro-thermal battery model is reorganized in a causal way to be coupled with the traction model of a commercial EV. The electrical part of the battery model is fully dependent on the battery internal temperature and the SOC [10].

Characterization tests are performed on one cell used in the studied EV. The battery parameters are thus obtained over a large temperature range (-5°C to 55 °C). This range corresponds to the EV use in temperate countries.

The electro-thermal model for one cell is validated at the component level in a thermal chamber with a programmable current supply. Then, the battery electro-thermal model is validated at the system level by comparison of the full EV simulation and on-board measurements during driving.

Finally, a driving range study highlights the interest of the electro-thermal model integration for EV simulation.

Not considering the electro-thermal coupling of the battery model (using a pure electrical battery model) overestimates the driving range by 2.5% at -5 °C ambient temperature and underestimates it by 2.5% at 40 °C. These values depend on the electric vehicle and the chosen driving cycle but the trend on driving range estimation remains.

The effect of battery thermal dependence can be coupled to the effect of the heating system in winter or air conditioning in summer. This model can be also used for studies on the impact of the battery preheating or any other thermal management [13] before driving.

The objective of this paper is not to obtain the best battery model but it is to enlight the impact of coupling a coupled battery electro-thermal model with an EV traction system. A driving range study is used to enlight the impact of the external temperature on the driving range but also on the traction current. The characterization tests have been made in a simple way and every parameters can be linked to physical phenomena and are stored in dynamic tables.

Nevertheless, more complex models for the battery and traction system can be investigated (more complex Thevenin models, thermal interractions between cells, cell parameters dispersion, variable contact resistance, efficiency map for machines..) at the cost of the computation time.

VII. Bibliography

[1] C. Dépature, W. Lhomme, A. Bouscayrol, P. Sicard, L. Boulon, "Efficiency map of the traction system of an electric vehicle from an on-road test drive", *IEEE Vehicle Power and Propulsion Conference*, Coimbra (Portugal), Oct. 2014.

[2] X. Li, C. Liu, et J. Jia, « Ownership and Usage Analysis of Alternative Fuel Vehicles in the United States with the 2017 National Household Travel Survey Data », *Sustainability*, vol. 11, no 8, p. 1-16, 2019.

[3] A. Cappetto et al., « Performance of wide temperature range electrolytes for Li-Ion capacitor pouch cells », *J. Power Sources,* vol. 359, p. 205-214, Aug. 2017.

[4] J. Jaguemont, L. Boulon, et Y. Dubé, « A comprehensive review of lithium-ion batteries used in hybrid and electric vehicles at cold temperatures », Appl. Energy, vol. 164, p. 99-114, Feb. 2016.

[5] J. P. Singer et K. P. Birke, « Kinetic study of low temperature capacity fading in Li-ion cells », *J. Energy Storage*, vol. 13, p. 129-136, Oct. 2017.

[6] J. Jaguemont, L. Boulon, P. Venet, Y. Dube, et A. Sari, « Lithium-Ion Battery Aging Experiments at Subzero Temperatures and Model Development for Capacity Fade Estimation », IEEE Transactions on Vehicular Technology, vol. 65, no 6, p. 4328-4343, June 2016.

[7] I. Baghdadi, O. Briat, J.-Y. Delétage, P. Gyan, et J.-M. Vinassa, « Lithium battery aging model based on Dakin's degradation approach », *J. Power Sources*, vol. 325, p. 273-285, Sept. 2016.

[8] C. Forgez, D. Vinh Do, G. Friedrich, M. Morcrette, et C. Delacourt, « Thermal modeling of a cylindrical LiFePO4/graphite lithium-ion battery », *J. Power Sources*, vol. 195, no 9, p. 2961-2968, May 2010.

[9] X. Hu, S. Lin, S. Stanton and W. Lian, "A Foster Network Thermal Model for HEV/EV Battery Modeling," in IEEE Transactions on Industry Applications, vol. 47, no. 4, pp. 1692-1699, July-Aug. 2011.

[10] J. Jaguemont, L. Boulon, et Y. Dubé, « Characterization and Modeling of a Hybrid-Electric-Vehicle Lithium-Ion Battery Pack at Low Temperatures », IEEE Transactions on Vehicular Technology, vol. 65, no 1, p. 1-14, Jan. 2016.

[11] H. E. Perez, X. Hu, S. Dey and S. J. Moura, "Optimal Charging of Li-Ion Batteries With Coupled Electro-Thermal-Aging Dynamics," in IEEE Transactions on Vehicular Technology, vol. 66, no. 9, pp. 7761-7770, Sept. 2017.

[12] W. Mohammed, E. Kamal, A. Aitouche and A. A. Sobaih, "Development Of Electro-Thermal Model of Lithium-Ion Battery for Plug-In Hybrid Electric Vehicles," 2018 7th International Conference on Systems and Control (ICSC), Valencia, 2018, pp. 201-206.

[13] J. Jaguemont, L. Boulon, Y. Dubé and F. Martel, "Thermal Management of a Hybrid Electric Vehicle in Cold Weather," in IEEE Transactions on Energy Conversion, vol. 31, no. 3, pp. 1110-1120, Sept. 2016.

[14] Y. Cao, R. C. Kroeze, et P. T. Krein, « Multi-timescale Parametric Electrical Battery Model for Use in Dynamic Electric Vehicle Simulations », *IEEE Transactions on Transportation Electrification,* vol. 2, no 4, p. 432-442, Dec. 2016.

[15] M. Amrhein and P. T. Krein, "Dynamic simulation for analysis of hybrid electric vehicle system and subsystem interactions, including power electronics," in IEEE Transactions on Vehicular Technology, vol. 54, no. 3, pp. 825-836, May 2005.

[16] L. Horrein, A. Bouscayrol, W. Lhomme, et C. Dépature, « Impact of Heating System on the Range of an Electric Vehicle », *IEEE Transactions on Vehicular Technology*, vol. 66, no 6, p. 4668-4677, June 2017.

[17] T. Yuksel and J. J. Michalek, "Effects of regional temperature on electric vehicle efficiency, range, and emissions in the united states," *Environmental Science and Technology*, vol. 49, no. 6, p. 3974–3980, 2015.

[18] K. Kambly, T. H Bradley, « Geographical and temporal differences in electric vehicle range due to cabin conditioning energy consumption", *Journal of Power Sources*, vol. 275, p. 468-475, Feb. 2015.

[19] S. Bellocchi, G. Leo Guizzi, M. Manno, M. Salvatori, and A. Zaccagnini, "Reversible heat pump HVAC system with regenerative heat exchanger for electric vehicles: Analysis of its impact on driving range," Applied Thermal Engineering, vol. 129, pp. 290–305, Jan. 2018.

[20] S. Gantenbein, M. Weiss, et E. Ivers-Tiffée, « Impedance based time-domain modeling of lithium-ion batteries: Part I », Journal of Power Sources, vol. 379, p. 317-327, Mar. 2018.

[21] R. German, A. Desreveaux and A. Bouscayrol, "Single Cell Electro-Thermal Model for Simulation of an Electric Vehicle," 2018 IEEE Vehicle Power and Propulsion Conference (VPPC), Chicago, IL, 2018, pp. 1-5.

[22] N. Omar,P. Van den Bossche,T. Coosemans, J. Van Mierlo, "Peukert Revisited—Critical Appraisal and Need for Modification for Lithium-Ion Batteries", Energies 2013, 6(11), 5625-5641.

[23] Elie RIVIERE, Ali SARI, Pascal VENET, Frederic MENIERE, Yann BULTEL, "Innovative Incremental Capacity Analysis Implementation for C / LiFePO4 Cell State-of-Health Estimation in Electrical Vehicles", Journal Batteries, vol. 5 (2), no. 37, April 1, 2019.

[24] P. Kreczanik, P. Venet, A. Hijazi, et G. Clerc, « Study of Supercapacitor Aging and Lifetime Estimation According to Voltage, Temperature, and RMS Current », *IEEE Trans. Ind. Electron*., vol. 61, no 9, p. 4895-4902, Sept. 2014.

[25] A. Bouscayrol, J.-P. Hautier, et B. Lemaire-Semail, «Systemic design methodologies for electrical energy systems-Chapter 3: Graphic formalism for the control of multi-physical energetic systems: COG and EMR», Wiley. New York, NY, USA, 2012.

[26] Tazzari Group, « Tazzari Zero use and maintainance manual », 2009.

[27] J. Lindgren et P. D. Lund, « Effect of extreme temperatures on battery charging and performance of electric vehicles », *Journal of Power Sources*, vol. 328, p. 37-45, Oct. 2016.

[28] E. Redondo-Iglesias, P. Venet, et S. Pelissier, « Global Model for Self-Discharge and Capacity Fade in Lithium-Ion Batteries Based on the Generalized Eyring Relationship », *IEEE Transactions on Vehicular Technology*, vol. 67, no 1, p. 104-113, Jan. 2018.

[29] Y. Wang, R. Pan, C. Liu, Z. Chen, et Q. Ling, « Power capability evaluation for lithium iron phosphate batteries based on multi-parameter constraints estimation », *J. Power Sources*, vol. 374, p. 12-23, Jan. 2018.

[30] T. T. Lou, W. G. Zhang, H. Y. Guo, et J. S. Wang, « The Internal Resistance Characteristics of Lithium-Ion Battery Based on HPPC Method », *Advanced Materials Research*, 2012.

[31] A. Berrueta, A. Urtasun, A. Ursúa, et P. Sanchis, « A comprehensive model for lithium-ion batteries: From the physical principles to an electrical model », *Energy*, vol. 144, p. 286-300, Feb. 2018.

[32] A. Castaings, W. Lhomme, R. Trigui, et A. Bouscayrol, « Practical control schemes of a battery/supercapacitor system for electric vehicle », *IET Electr. Syst. Transp.*, vol. 6, no 1, p. 20-26, 2016.

[33] X. Lin et al., « Online Parameterization of Lumped Thermal Dynamics in Cylindrical Lithium Ion Batteries for Core Temperature Estimation and Health Monitoring », *Control Syst. Technol. IEEE Trans. On*, vol. 21, no 5, p. 1745-1755, Sept. 2013.

Appendix A: EMR Pictograms

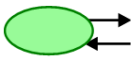	Source element (energy source)	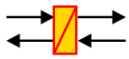	Accumulation element (energy storage)	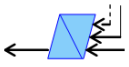	Indirect inversion (closed-loop control)
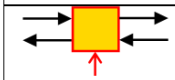	Mono-physical conversion element	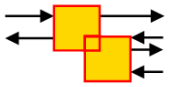	Mono-physical coupling element (energy distribution)	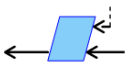	Direct inversion (open-loop control)
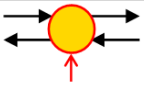	Multi-physical conversion element	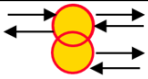	Multi-physical coupling element (energy distribution)	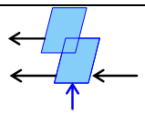	Coupling inversion (energy criteria)